Research on Chemical Intermediates (2023) 49:3065–3078
https://doi.org/10.1007/s11164-023-05029-z

Novel $S_2O_8^{2-}$/Fe-ZrO_2 solid superacid catalyst combined with O_2-Ac_2O for highly efficient catalytic nitration of 1-nitronaphthalene with NO_2 to 1,5-dinitronaphthalene

Jiaqi Yan[1] · Xiaowen Zhang[2,4] · Jiahong Yin[2] · Fangfang Zhao[2] · Kuiyi You[2,3] · He'an Luo[2,3]

Received: 11 February 2023 / Accepted: 5 May 2023 / Published online: 13 May 2023
© The Author(s), under exclusive licence to Springer Nature B.V. 2023

Abstract

A mild, efficient, and green approach for highly selective synthesis of 1,5-dinitronaphthalene (1,5-DNN) has been devolved from catalytic nitration of 1-nitronaphthalene (1-NN) with NO_2 combined with O_2-Ac_2O over solid superacid $S_2O_8^{2-}$/Fe-ZrO_2. The prepared $S_2O_8^{2-}$/Fe-ZrO_2 catalyst presents better catalytic performance than most of the reported catalysts for this purpose, with 96.8% conversion of 1-NN and 62.6% selectivity of 1,5-DNN under the optimized reaction conditions. The excellent catalytic activity of $S_2O_8^{2-}$/Fe-ZrO_2 can be attributed to its remarkable Lewis acid sites and strong acidity. A possible catalytic nitration reaction pathway of 1-NN with NO_2 over $S_2O_8^{2-}$/Fe-ZrO_2 in the O_2-Ac_2O system was proposed. This work provides a practical strategy for the cost-effective, environmentally friendly, and efficient synthesis of 1,5-DNN with significant industrial application prospects.

Keywords Solid superacid · Nitration reaction · 1,5-Dinitronaphthalene · 1-Nitronaphthalene · Nitrogen dioxide

✉ Xiaowen Zhang
xzhang1@xtu.edu.cn

✉ Kuiyi You
kuiyiyou@xtu.edu.cn

[1] Furong College, Hunan University of Arts and Science, Changde 415000, People's Republic of China

[2] School of Chemical Engineering, Xiangtan University, Xiangtan 411105, People's Republic of China

[3] National & Local United Engineering Research Center for Chemical Process Simulation and Intensification, Xiangtan University, Xiangtan 411105, People's Republic of China

[4] Foshan Green Intelligent Manufacturing Research Institute of Xiangtan University, Foshan 528311, People's Republic of China

Introduction

Aromatic compound nitration is a significant industrial process for the production of chemical intermediates [1, 2]. In particular, nitration of 1-nitronaphthalene (1-NN) or naphthalene yields dinitronaphthalenes (1,5-DNN, 1,8-DNN, 1,3-DNN, and 1,4-DNN), which can be used to make polyurethanes, plastics, and dyes [3]. 1,5-DNN, for example, is an important raw material for the preparation of intermediate polyurethanes and 1,5-naphthalene diisocyanate [4]. Because 1,5-DNN is the most commercially valuable and in-demand dinitronaphthalene product, considerable studies are devoted to boosting its output. The typical approach for preparing 1,5-DNN involves nitration of 1-NN or naphthalene, which is usually catalyzed by significant volumes of concentrated H_2SO_4 and HNO_3. However, this method has unavoidable drawbacks, such as low selectivity (30–35%), extensive energy requirement, high corrosion, and negative environmental effect [5, 6]. As a result, it is necessary to develop a benign and economically feasible nitration approach to increase the selectivity of 1,5-DNN and improve the notorious production environment.

Solid acid catalysts for the nitration of 1-NN or naphthalene have recently attracted growing attention as a way to make dinitronaphthalene more cleanly and with higher selectivity. Various solid acid catalysts have been reported for this purpose, such as acid-treated clay [7], ionic liquid-based catalysts [8–10], modified zeolites [11, 12], and sulfated metal oxides (SO_4^{2-}/M_xO_y) [13–15]. Nevertheless, the process still produces large quantities of undesirable by-products, consumes too much concentrated HNO_3 as a nitrating agent, or obtains low target selectivity. This has motivated the study of eco-friendly nitrating agents to obtain a high selectivity of 1,5-DNN. Mascal et al. found that when [Ag-K-Na] NO_3 is used as a nitrating agent, the selectivity of 1,5-DNN for the nitration of naphthalene under the catalysis of $K_3Fe(CN)_6$ was only 2.1% [16]. According to Wang et al., the selectivity of 1,5-DNN was 56% for the nitration of 1-NN with the NO_2-O_2 system using a zeolite catalyst [17]. Our previous work demonstrated that when 1-NN was nitrated with NO_2 employing a HY catalyst, the selectivity of 1,5-DNN was 35% [12]. Consequently, it is of great significance to develop high-efficiency catalysts for clean and green nitration processes under facile conditions.

Among solid acid catalysts, the SO_4^{2-}/M_xO_y catalyst has been widely evaluated for many acid catalytic reactions, such as isomerization, alkylation, acetalization, and nitration reactions, due to its easy synthesis, good thermal stability, and super acidity [18–21]. Jiao et al. presented a solvent-free liquid phase toluene nitration process, utilizing NO_2 as the nitrifying agent and SO_4^{2-}/WO_3 as the catalyst, which exhibited good catalytic activity [13]. Yan et al. observed that catalyzing the nitration of 1-NN with NO_2 and SO_4^{2-}/ZrO_2 resulted in 93.8% 1-NN conversion and 52.8% 1,5-DNN selectivity [14]. Based on the literature, transition metal-modified SO_4^{2-}/M_xO_y catalysts can significantly enhance catalytic performance. $CuO/SO_4^{2-}/ZrO_2$, for example, was shown by Occelli et al. to have better catalytic performance and stability than SO_4^{2-}/ZrO_2 [22]. After the inclusion

of Pd and Co metals, Córdoba et al. discovered that the lifetime of SO_4^{2-}/ZrO_2 in NO_x reduction by methane was extended [23]. In the nitration of aromatic compounds, Wang et al. revealed that TiO_2-Fe_3O_4-SO_4^{2-}/ZrO_2 presented higher catalytic activity than SO_4^{2-}/ZrO_2, possibly due to the synergistic interaction between metal oxides [24]. Using Fe- and Mn-modified SO_4^{2-}/ZrO_2 catalyzed nitration of 1-NN with NO_2 driven by O_2-Ac_2O, our previous work indicated that 92.6% conversion to 1-NN and 57.2% selectivity to 1,5-DNN were achieved [25].

On the other hand, in comparison with SO_4^{2-}, $S_2O_8^{2-}$ is easier to coordinate with metal oxides, which can provide more superacid sites and sulfur active components to enhance catalytic performance [26–28]. Moreover, compared with the H_2SO_4, $(NH_4)_2S_2O_8$ is a safe acidifying agent during the preparation of the catalyst (impregnation process). The previous work considered that $S_2O_8^{2-}/M_xO_y$ presented stronger acidity, higher catalytic effect, and stability than SO_4^{2-}/M_xO_y [29–31]. It is therefore of great interest to adopt the metal oxide promoted $S_2O_8^{2-}/ZrO_2$ catalyst for the liquid phase nitration of 1-NN with NO_2 assisted by O_2-Ac_2O to make this process more environmentally and economically feasible. To the authors' knowledge, the use of Fe-modified $S_2O_8^{2-}/ZrO_2$ in the nitration of the 1-NN process has rarely been reported heretofore.

Experimental section

Materials

The materials employed in this study are presented in supplementary information (SI).

Catalyst synthesis

The coprecipitation–impregnation method was used to prepare the Fe-modified $S_2O_8^{2-}/ZrO_2$ catalyst ($S_2O_8^{2-}$/Fe-ZrO_2), and the regenerated $S_2O_8^{2-}$/Fe-ZrO_2 catalyst means that the catalyst was washed, dried, and then calcined at 600 °C after being recycled for five times. Details are displayed in SI.

Catalyst characterization

The catalysts were characterized by X-ray diffraction (XRD), Fourier transform infrared spectroscopy(FT-IR), N_2 adsorption/desorption experiment, inductively coupled plasma-optical emission spectrometer (ICP-OES), scanning electron microscope (SEM), high-resolution transmission electron microscope (HRTEM), X-ray photoelectron spectroscopy (XPS), temperature programmed desorption of ammonia (NH_3-TPD), and pyridine adsorption infrared spectroscopy (Py-FT-IR). Detailed information about these methods is available in SI.

Typical experimental process

The catalytic nitration of 1-NN with the NO_2 test was performed based on the method reported in our previous work [14, 25], and detailed information about this test is listed in SI.

Results and discussion

Catalytic performance of different catalysts

Several typical solid superacid catalysts were evaluated under the same reaction conditions to find an efficient catalyst for the nitration of 1-NN with NO_2 aided by O_2-Ac_2O, and the results are tabulated in Table 1. For the non-catalytic reaction, the nitration of 1-NN with NO_2 assisted by acetic anhydride (Ac_2O) could result in the formation of 1,5-DNN, and 16.1% of 1-NN conversion with 39.9% selectivity to 1,5-DNN was obtained. When O_2 was introduced into the nitration reaction, the conversion of 1-NN increased to 83.9%, and the selectivity of 1,5-DNN was 40.7%. Stabilization of NO_2^+ and formation of an active acetyl nitrate ($AcONO_2$) nitrating reagent are thought to be responsible for the beneficial effect of Ac_2O on enhancing reaction activity.

Regarding the catalytic reaction process, all tested solid superacid catalysts $S_2O_8^{2-}/M_xO_y$ improved catalytic activity in the metal oxides and non-catalytic

Table 1 Comparison of the catalytic nitrification performance of different systems

Catalyst	Nitration system	Conversion (%)	Selectivity (%)		
			1,5-DNN	1,8-DNN	Others
–	NO_2-CH_3CN	0	0	0	0
–	NO_2-$C_2H_4Cl_2$	0	0	0	0
–	NO_2-$C_2H_4O_2$	0	0	0	0
–	NO_2-Ac_2O	16.1	39.9	35.9	24.2
–	NO_2-O_2-Ac_2O	83.9	40.7	29.4	29.9
ZrO_2	NO_2-O_2-Ac_2O	87.6	45.6	26.6	27.8
CuO	NO_2-O_2-Ac_2O	80.0	45.3	41.0	14.7
Fe_2O_3	NO_2-O_2-Ac_2O	86.9	38.2	26.8	35.0
$S_2O_8^{2-}/ZrO_2$	NO_2-O_2-Ac_2O	95.3	47.6	35.5	16.9
$S_2O_8^{2-}/CuO$	NO_2-O_2-Ac_2O	86.2	42.1	35.5	22.4
$S_2O_8^{2-}/Fe_2O_3$	NO_2-O_2-Ac_2O	90.8	45.4	33.2	21.4
$S_2O_8^{2-}/Cu$-ZrO_2	NO_2-O_2-Ac_2O	95.5	48.7	34.5	16.8
$S_2O_8^{2-}/Fe$-ZrO_2	NO_2-O_2-Ac_2O	94.9	53.4	23.6	23.0
$S_2O_8^{2-}/Fe$-ZrO_2 [b]	NO_2-O_2-Ac_2O	96.8	62.6	20.7	16.7

Reaction conditions: the molar ratio of 1-NN to NO_2 is 1:4, 35 °C, 0.5 MPa O_2, 4 h, catalyst dosage 0.5 g, solvent 10.0 g. [b] The molar ratio of 1-NN to NO_2 is 1:3, 40 °C, 0.7 MPa O_2, 5 h, catalyst dosage 0.5 g, solvent 10.0 g

process, with $S_2O_8^{2-}$/ZrO_2 exhibiting the highest catalytic performance with a selectivity of 47.6% to 1,5-DNN. On the other hand, the use of metal oxide-modified $S_2O_8^{2-}$/ZrO_2 catalysts greatly improved reaction activity, and the Fe-modified solid superacid catalyst, $S_2O_8^{2-}$/Fe-ZrO_2 improved catalytic performance even more with 53.4% selectivity of 1,5-DNN. $S_2O_8^{2-}$/Fe-ZrO_2 was found to have the highest catalytic activity, resulting in 96.8% conversion of 1-NN and 62.6% selectivity of 1,5-DNN under optimal reaction conditions (Sect. 3.2).

Optimization of catalyst preparation conditions

In order to further improve its catalytic performance, the preparation conditions of the $S_2O_8^{2-}$/Fe-ZrO_2 catalyst that included the mass fraction of Fe_2O_3, the concentration of the acidifying reagent $(NH_4)_2S_2O_8$, and the calcination temperature were optimized. The results for the nitration of 1-NN are depicted in Fig. S1. Figure S1(a) presents the catalytic performance of $S_2O_8^{2-}$/Fe-ZrO_2 with various contents of Fe_2O_3. When the iron content is 2 wt%, the selectivity of 1,5-DNN is highest at 53.4%, and the conversion of 1-NN is 94.9%.

The influence of varied $(NH_4)_2S_2O_8$ impregnation concentrations on 1-NN nitration is displayed in Fig. S1(b). The selectivity of 1,5-DNN decreases significantly as the impregnation concentration lowers, which is due to a reduction in acid content, a reduction in the quantity of acid supported by the catalyst, and a decrease in catalytic efficiency. However, the catalytic performance is lower than that of 0.5 M when the concentration is 1 M. This might be related to excessive $(NH_4)_2S_2O_8$ that cannot be properly supported on the carrier surface, the reduction of the number of metal oxide particles on the catalyst surface, and the formation of persulfate salts that cover the surface activity sites of the catalyst [32]. As a result, a concentration of $(NH_4)_2S_2O_8$ of 0.5 M is preferred.

As shown in Fig. S1(c), the catalyst exhibits the best catalytic activity when the calcination temperature is 600 °C, with a selectivity of 1,5-DNN of 53.4%. With a change in the calcination temperature, the catalytic performance has an obvious trend of change. This is because the lower calcination temperature cannot allow ZrO_2 to form a relatively complete tetragonal phase, which is not conducive to the formation of stable acid sites. When the calcination temperature is too high, sulfur combined with the catalyst will be lost and the tetragonal phase will be weakened, resulting in the loss of the surface-active centers [33]. Accordingly, the optimized calcination temperature is 600 °C.

Optimization of reaction conditions and stability of the catalyst

The $S_2O_8^{2-}$/Fe-ZrO_2 catalyst obtained under optimized preparation conditions, that is, the iron content of 2 wt%, an acid treatment concentration of 0.5 mol/L, and a calcination temperature of 600 °C, was used for further studies. Reaction factors, including the molar ratio of 1-NN to NO_2, reaction temperature, oxygen pressure, reaction time, and catalyst dosage were optimized for the nitration of 1-NN with the prepared $S_2O_8^{2-}$/Fe-ZrO_2 catalyst, and the results are displayed in Fig. 1a–e.

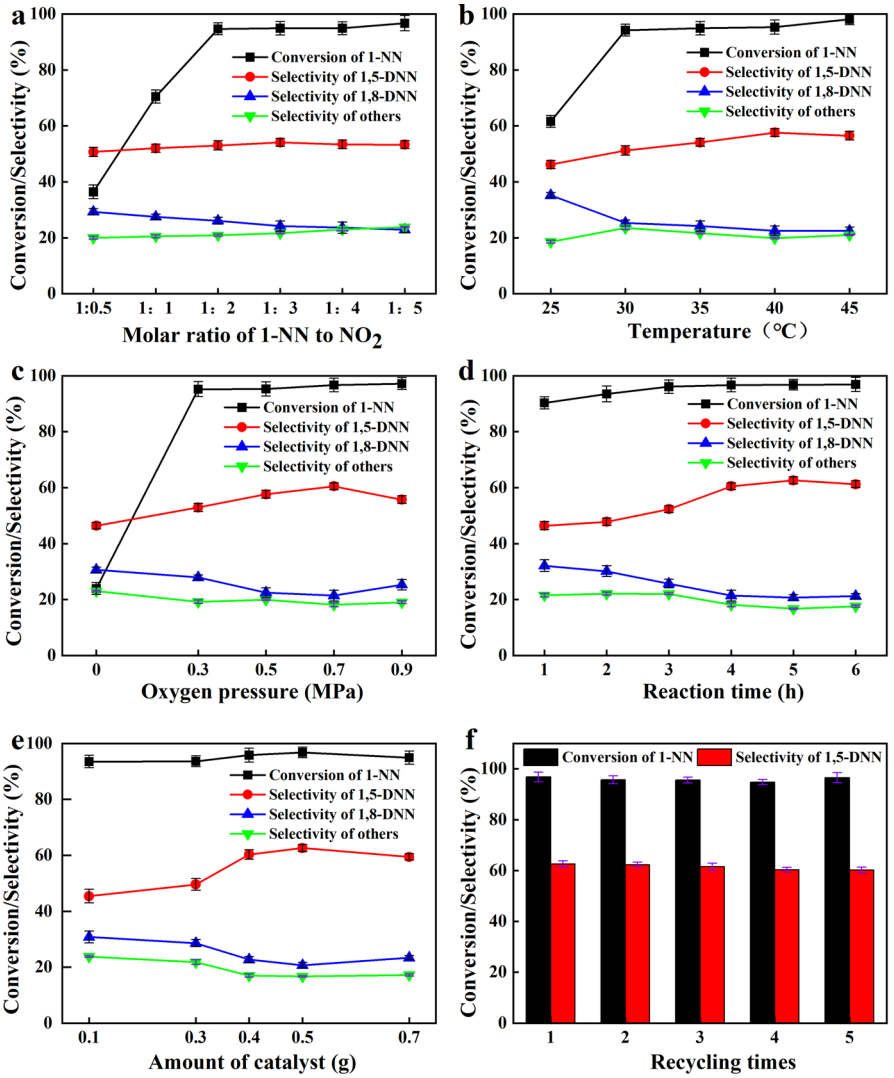

Fig. 1 Effects of parameters on the nitration reaction. Reaction condition: **a** 35 °C, 0.5 MPa O_2, 4 h, catalyst dosage 0.5 g, solvent 10.0 g; **b** 1-NN to NO_2 is 1:3, 0.5 MPa O_2, 4 h, catalyst dosage 0.5 g, solvent 10.0 g; **c** 1-NN to NO_2 is 1:3, 40 °C, 4 h, catalyst dosage 0.5 g, solvent 10.0 g; **d** 1-NN to NO_2 is 1:3, 40 °C, 0.7 MPa O_2, catalyst dosage 0.5 g, solvent 10.0 g; **e** 1-NN to NO_2 is 1:3, 40 °C, 0.7 MPa O_2, 5 h, solvent 10.0 g. **f** Cyclic tests of the $S_2O_8^{2-}$/Fe-ZrO_2 catalyst. Reaction conditions: 1-NN to NO_2 is 1:3, 40 °C, 0.7 MPa O_2, 5 h, catalyst dosage 0.5 g, solvent 10.0 g

The impact of the molar ratio of 1-NN to NO_2 is given in Fig. 1a. Note that the conversion of 1-NN is increased with increased content of NO_2, and when 1-NN/NO_2 was 1:3, the selectivity of 1,5-DNN reaches the highest value. Similarly, as shown in Fig. 1b–d, the reaction temperature, oxygen pressure, and reaction time present similar change trends and results. The effect of the amount of catalyst on

the nitration reaction results is depicted in Fig. 1e. It can be seen that a suitable amount of $S_2O_8^{2-}$/Fe-ZrO_2 catalyst is favorable for the formation of 1,5-DNN. Consequently, the optimization factors are obtained: the molar ratio of 1-NN to NO_2: 1:3, reaction temperature: 40 °C, partial pressure of O_2: 0.7 MPa, reaction time: 5 h, and catalyst dosage: 0.5 g. Under these reaction conditions, 96.8% 1-NN conversion with 62.6% 1,5-DNN selectivity is achieved over the $S_2O_8^{2-}$/Fe-ZrO_2 catalyst.

The stability of $S_2O_8^{2-}$/Fe-ZrO_2 catalyst for the catalytic 1-NN nitration reaction was evaluated under the optimized reaction conditions, and the results are displayed in Fig. 1f. For the cyclic tests, after the catalytic reaction was finished, the spent catalyst was filtered, washed, dried, and then used for the next cycle test. After the catalyst was recycled five times, the conversion of 1-NN did not change and the selectivity of 1,5-DNN decreased only by 3.8% (62.6% to 60.2%). Furthermore, as demonstrated in Sect. 3.4, the characterization results (XRD, FT-IR, N_2 adsorption–desorption experiment, and ICP-OES) revealed that the structure, composition, and acidity of the regenerated catalyst hardly changed after five cycles. These results demonstrated that the $S_2O_8^{2-}$/Fe-ZrO_2 catalyst had outstanding recyclability for the nitration of 1-NN.

Meanwhile, comparison of catalytic activities in the nitration of 1-NN with various reported catalysts and nitration systems is summarized in Table 2. Compared with treated clay, metal salt, and ionic liquids-based catalysts, $S_2O_8^{2-}$/Fe-ZrO_2 has excellent recyclability. The NO_2-O_2-Ac_2O nitration system is more environmentally friendly than the concentrated HNO_3 as nitrating agent. Furthermore, the catalytic activity of the $S_2O_8^{2-}$/Fe-ZrO_2 catalyst is better than most of the reported solid acid catalysts for the nitration of 1-NN (Table 2). Accordingly, the combination of the $S_2O_8^{2-}$/Fe-ZrO_2 catalyst and the NO_2-O_2-Ac_2O nitration system provides a practical

Table 2 Comparison of the results of 1-NN or naphthalene nitration in different nitration systems

Catalyst	Nitration system	*T* (°C)	Time (h)	1-NN or naphthalene Conversion (%)	1,5-DNN Selectivity (%)	Refs.
Fuming H_2SO_4	65% HNO_3	40–80	–	> 99.0 (naphthalene)	~ 35.0	[34]
$K_3Fe(CN)_6$	$Ag_{0.51}K_{0.42}Na_{0.07}NO_3$	160	1	– (naphthalene)	2.1	[16]
Claycop	HNO_3-Ac_2O-CCl_4	–	3	97.0 (naphthalene)	23.0	[7]
$Ni(CH_3COO)_2{\cdot}4H_2O$	NO_2-AN	100	3	33.1 (1-NN)	34.1	[35]
HY	NO_2-CH_3CN	90	4	42.8 (1-NN)	35.7	[12]
$[C_5H_5NMe]^+HSO_4^-$	98% HNO_3	–	–	– (naphthalene)	38.0	[36]
PW/HZSM-5	65% HNO_3	65	3	100.0 (naphthalene)	48.5	[37]
LaZSM-5	NO_2-O_2-CH_3CN	85	48	50.0 (1-NN)	56.0	[17]
SO_4^{2-}/FeMn-ZrO_2	NO_2-O_2-Ac_2O	35	4	92.6 (1-NN)	57.2	[25]
HY	HNO_3-CH_3NO_2	78	4	99.0 (1-NN)	57.9	[38]
$S_2O_8^{2-}$/Fe-ZrO_2	NO_2-O_2-Ac_2O	40	5	96.8 (1-NN)	62.6	This work

pathway for the low-cost, efficient and green synthesis of 1,5-DNN with great potential for industrial application.

Results of catalyst characterization

Figure 2a displays the XRD patterns of fresh, used, and regenerated $S_2O_8^{2-}$/Fe-ZrO_2 catalysts. Note that all patterns show the same diffraction peaks at 2 thetas of 30.1, 35.2, 50.2, and 60.2°, which can be assigned to the pure tetragonal phase ZrO_2 (JCPDS No. 88–1007) [39]. The non-appearance of diffraction reflection of iron oxides suggests that these oxides are well dispersed on the surface or may migrate evenly into the interior of the ZrO_2 tetragonal phase lattice [40]. Moreover, after the catalyst was used five times, the crystal phase structure of the catalyst remains unchanged.

FT-IR spectra of catalysts are presented in Fig. 2b. Bands around 545 cm^{-1} are attributed to the characteristic peak of crystalline ZrO_2 [41]. Peaks at around 3440 and 1632 cm^{-1} refer to the H–O-H bending frequency of adsorbed water [42]. Two peaks at about 1270 and 1074 cm^{-1} can be assigned to chelating bidentate persulfate groups coordinated with the surface of the metal oxide supports [43]. These results indicated that the persulfate group has been successfully bonded to the supports.

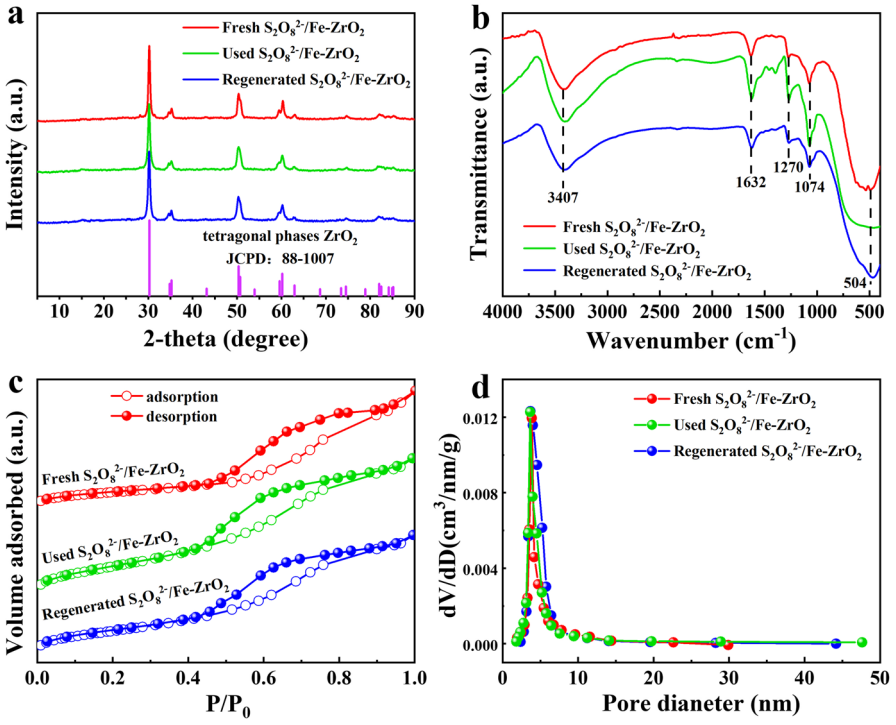

Fig. 2 Catalyst characterization results. **a** XRD patterns. **b** FT-IR spectra. **c** N_2 adsorption–desorption isotherms. **d** Pore diameter distributions

Furthermore, the regenerated catalyst presents peaks similar to those of the fresh $S_2O_8^{2-}$/Fe-ZrO_2 catalyst, demonstrating that the framework of the catalyst remained intact after five catalytic reaction cycles.

Figure 2c, d presents the isotherms of the N_2 adsorption–desorption and pore diameter distribution curves of the fresh, used, and regenerated $S_2O_8^{2-}$/Fe-ZrO_2 catalysts. Table 3 tablets the textural properties of the samples. It can be seen that the three samples present the same type IV isotherms with a H2 type hysteresis loop ($P/P_0 = 0.4–1.0$), belonging to the feature of the mesoporous structure [44, 45]. Compared with the pure ZrO_2, the surface area of $S_2O_8^{2-}$/Fe-ZrO_2 increases, while the pore diameter decreases after acidification with ammonium persulfate. $S_2O_8^{2-}$/Fe-ZrO_2 exhibits better textural properties factors than the ZrO_2 catalyst, including surface area, pore volume, and pore diameter. In addition, the structural properties of $S_2O_8^{2-}$/Fe-ZrO_2 decreased slightly after five recycles, while the structural factors of spent $S_2O_8^{2-}$/Fe-ZrO_2 can be regenerated by calcination.

The morphology of the fresh $S_2O_8^{2-}$/Fe-ZrO_2 catalyst was researched by SEM (Fig. 3a) and HRTEM (Fig. 3b, c). As shown in Fig. 3a, the $S_2O_8^{2-}$/Fe-ZrO_2 surface is rough and uneven particles are deposited into large congeries. The TEM image (Fig. 3b) reveals the morphology of the crystal, which is agglomerated by uneven nano-crystalline particles (Fig. 3b, c). Moreover, the HRTEM image (Fig. 3c) of the $S_2O_8^{2-}$/Fe-ZrO_2 catalyst shows two distinct lattices spacing about 0.295 nm and 0.252 nm, which can be attributed to the (101) and (110) lattice planes of the tetragonal phase ZrO_2, respectively [46]. Unfortunately, the lattice spacing of iron oxide was not found in the HRTEM image, possibly due to the low additional amount.

XPS can be utilized to analyze the chemical state of elemental species in the $S_2O_8^{2-}$/Fe-ZrO_2 catalyst [47]. The XPS measurement results are shown in Fig. 4. As shown in Fig. 4a, the banding energy gap between Zr 3d 5/2 and Zr 3d 3/2 is higher than 2.3 eV, suggesting that the Zr species are primary in the Zr^{4+} form in the catalyst [48]. The peaks at 184.2 (3d 3/2) and 181.8 eV (3d 5/2) correspond to the Zr-O-Zr bond of ZrO_2 [49]. Bands at 184.8 (3d 3/2) and 182.3 eV (3d 5/2) are due to the Zr-O-S bond [50]. For the O 1 s spectrum of a catalyst (Fig. 4b), the peaks at about 529.7, 531.3, and 532.1 eV represent the binding energies of the O-Zr bond (ZrO_2), the O-S bond (persulfate group), and the O–H bond (surface hydroxyl group), respectively [51, 52]. The O 1 s peak for Fe–O has not appeared from the XPS result, which may be attributed to the content of iron is low. For the

Table 3 Textural properties of catalysts

Samples	Surface area (m^2/g)	Pore volume (cm^3/g)	Pore diameter (nm)	Composition (wt.%)	
				S	Fe
ZrO_2	48.6	0.13	10.64	–	–
Fresh $S_2O_8^{2-}$/Fe-ZrO_2	88.4	0.10	4.4	2.63	1.91
Used $S_2O_8^{2-}$/Fe-ZrO_2	83.8	0.09	4.2	2.54	1.78
Regenerated $S_2O_8^{2-}$/Fe-ZrO_2	86.2	0.09	4.3	2.48	1.72

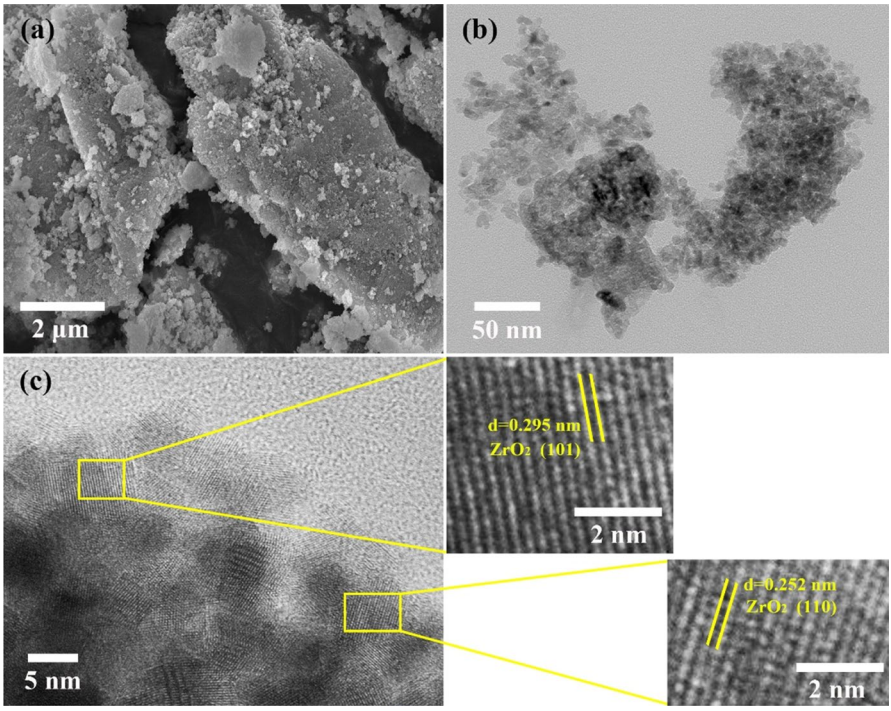

Fig. 3 The morphology of the $S_2O_8^{2-}$/Fe-ZrO_2 catalyst. **a** SEM image. **b** and **c** TEM and HRTEM images

S 2p spectrum, as shown in Fig. 4c, the peak at around 167–172 eV is attributed to the S^{6+} element, which can be separated into two bands at 169.9 and 168.7 eV [25]. The peak at 168.7 eV is due to the deprotonated persulfate groups, while the band at 169.9 eV is due to the protonated groups [53]. In the Fe 2p spectrum (Fig. 4d), the peak at 718.3 eV is the satellite peak of Fe. Peaks at around 711.3 and 724.8 eV are related to the binding energies of Fe 2p 3/2 and Fe 2p 1/2, respectively. The binding energy gap between Fe 2p 3/2 and Fe 2p 1/2 is greater than 13 eV, demonstrating that Fe species exist mainly in the form of Fe^{3+} in the $S_2O_8^{2-}$/Fe-ZrO_2 catalyst [42, 54]. The XPS results demonstrate that the persulfate groups have bonded to Fe-modified ZrO_2, and Fe^{3+} exists in the $S_2O_8^{2-}$/Fe-ZrO_2 catalyst.

The acid types, Brønsted acid sites (B acid site) and Lewis acid sites (L acid site) of the ZrO_2 and $S_2O_8^{2-}$/Fe-ZrO_2 catalysts were measured using pyridine-FT-IR, and the results are given in Fig. 5a. Generally, for the pyridine-FT-IR spectra, the band at around 1449 and 1608 cm^{-1} can be attributed to the L acid sites, and the band at about 1544 cm^{-1} can be ascribed to B acid sites [48]. The peak at 1486 cm^{-1} is related to both B acid sites and L acid sites [45]. Compared to pure ZrO_2, which only possesses a small amount of L acid sites, the $S_2O_8^{2-}$/Fe-ZrO_2 catalyst has both B and L acid sites, while the L acid site is dominant. The abundant L acid sites of the $S_2O_8^{2-}$/Fe-ZrO_2 catalyst may be one of the reasons for its excellent catalytic activity for the nitration of 1-NN.

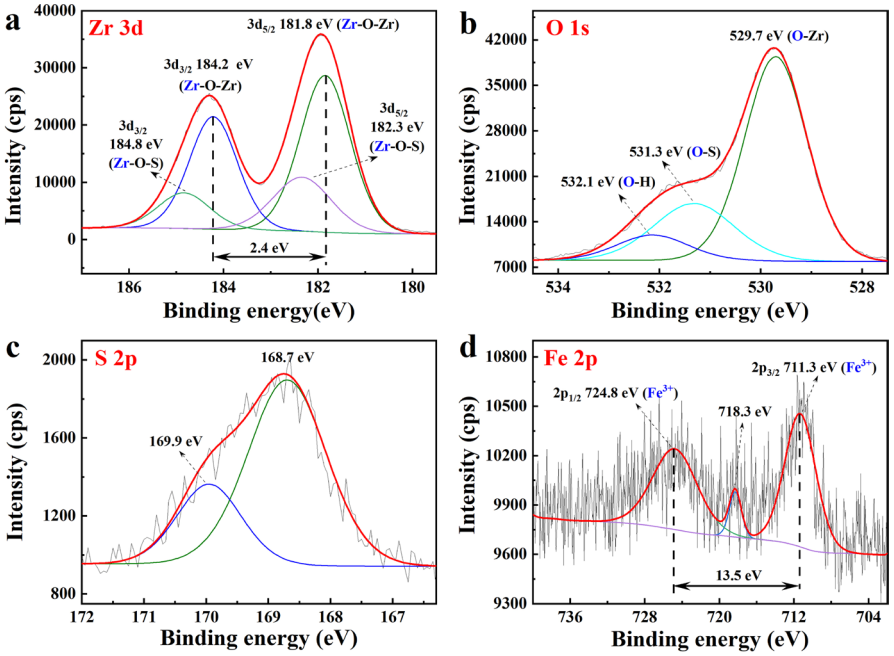

Fig. 4 XPS spectra of the $S_2O_8^{2-}$/Fe-ZrO_2 catalyst. **a–d** Zr 3d, O 1S, S 2p, and Fe 2p spectra, respectively

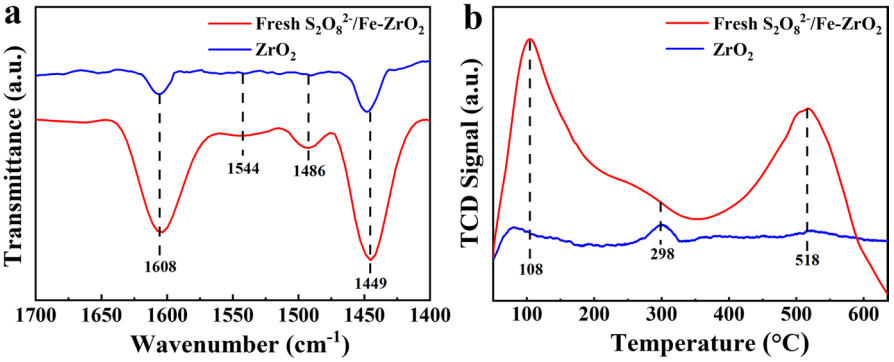

Fig. 5 Results of catalyst acidity characterization. **a** Pyridine adsorbed FT-IR spectra. **b** NH_3-TPD curves

NH_3-TPD results of fresh $S_2O_8^{2-}$/Fe-ZrO_2 and pure ZrO_2 catalysts are presented in Fig. 5b. Regarding NH_3-TPD measurement results, acid sites can be divided into weak (< 200 °C), medium (200–400 °C), and strong acid sites (> 400 °C) according to the desorption temperature of NH_3 [44, 48]. According to Fig. 5b, pure ZrO_2 only possesses a few weak and medium–strong acid sites. However, as shown in Fig. 5b, the broad NH_3-TPD desorption curve of the $S_2O_8^{2-}$/Fe-ZrO_2 catalyst demonstrates that the acid sites are widely distributed and that the weak, medium, and strong acid

sites coexist. $S_2O_8^{2-}$/Fe-ZrO_2 has a higher acid strength than pure ZrO_2, especially for strong acid sites. Therefore, the strong acid sites may be one of the most important factors determining the catalytic nitration performance of the catalyst.

Catalytic mechanism

Figure 6 gives the possible mechanism of nitration 1-NN over the $S_2O_8^{2-}$/Fe-ZrO_2 catalyst in the O_2-Ac_2O system. During the NO_2 and O_2 reaction, there is an oxidation process that might release the resultant $NO_2^+ \cdot NO_3^-$ species [11, 55], and the liberated $NO_2^+ \cdot NO_3^-$ can react with Ac_2O to form $AcONO_2$, which is then adsorbed on the acid site of the catalyst, resulting in the formation of an acetyl nitrate cation ($AcONO_2^+$) [25]. The electrophilic species $AcONO_2^+$ is likely to assault 1-NN to generate the Wheland intermediate and release acetic acid [11]. Finally, the $S_2O_8^{2-}$/Fe-ZrO_2 catalyst is recovered by acquiring a proton from the intermediate and nitration products are also achieved.

Conclusions

In summary, an effective and environmentally friendly method has been reported to prepare a high 1,5-DNN selectivity from the nitration of 1-NN with NO_2 aided by O_2-Ac_2O using a $S_2O_8^{2-}$/Fe-ZrO_2 catalyst. The findings demonstrate that the $S_2O_8^{2-}$/Fe-ZrO_2 catalyst and O_2-Ac_2O play an important role in the synthesis of 1,5-DNN. The $S_2O_8^{2-}$/Fe-ZrO_2 catalyst possesses high Lewis acid sites and strong acidity, thus exhibiting excellent catalytic activity and stability. 96.8% conversion of 1-NN and 62.6% selectivity of 1,5-DNN were achieved under optimal conditions. Compared to the previously reported catalyst for the nitration of 1-NN, the $S_2O_8^{2-}$/

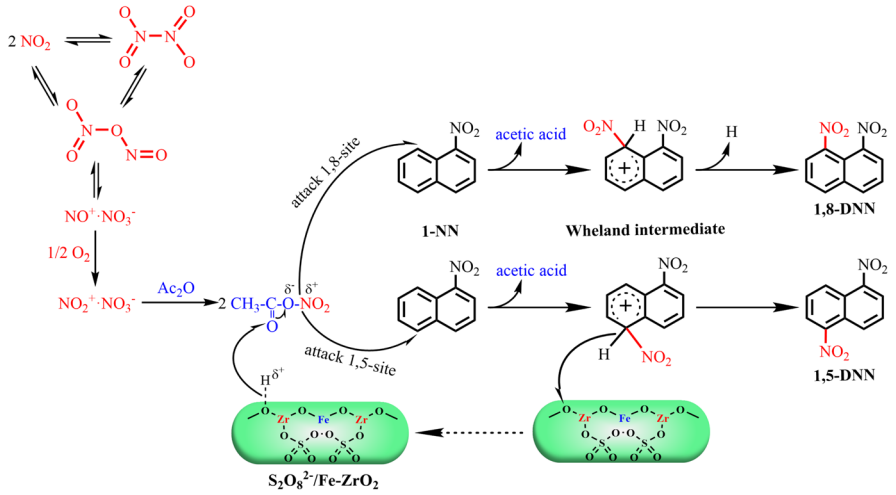

Fig. 6 Possible nitration mechanism of 1-NN with NO_2 over $S_2O_8^{2-}$/Fe-ZrO_2 in the O_2-Ac_2O system

Fe-ZrO_2 catalyst presents greater catalytic activity. The well-developed 1-NN nitration process for the creation of valuable 1,5-DNN, which uses NO_2 as a benign nitrating agent instead of HNO_3 and $S_2O_8^{2-}$/Fe-ZrO_2 as a solid acid catalyst instead of H_2SO_4, has significant promise for real-world applications.

Supplementary Information The online version contains supplementary material available at https://doi.org/10.1007/s11164-023-05029-z.

Author contributions Jiaqi Yan: Data curation, Validation, Formal analysis, Writing-original draft. Xiaowen Zhang: Supervision, Formal analysis, Writing-original draft, Funding acquisition. Jiahong Yin: Data curation, Validation, Formal analysis. Fangfan Zhao: Formal analysis, Funding acquisition. Kuiyi You: Conceptualization, Supervision, Revision, Data curation. He'an Luo: Conceptualization, Supervision.

Funding This work was supported by the National Natural Science Foundation of China (22208271), Science and Technology Innovation Program of Hunan Province (2021RC2089), Guangdong Basic and Applied Basic Research Foundation (2021A1515110136), Research fund of Hunan Provincial Education Department (20B550).

Data availability The authors confirm that the data supporting the findings of this study are available within the article.

Declarations

Conflict of interest The authors declare that they have no competing interests.

Ethical approval Not applicable for this work.

References

1. K. Muto, T. Okita, J. Yamaguchi, ACS Catal. **10**, 9856 (2020)
2. M. Kashihara, Y. Nakao, Acc. Chem. Res. **54**, 2928 (2021)
3. S.-Y. Hong, S.-M. Park, J. Electrochem. Soc. **150**, 360 (2003)
4. W. Xiong, K.-J. Wang, X.-W. Liu, F. Hao, H.-Y. Xiao, P.-L. Liu, H.-A. Luo, Appl. Catal. A Gen. **514**, 126 (2016)
5. G.A. Olah, S.C. Narang, J.A. Olah, Proc. Natl. Acad. Sci. USA **78**, 3298 (1981)
6. W. Xiong, S. Zhou, Z. Zhao, F. Hao, Z. Cai, P. Liu, H. Zhang, H. Luo, Front. Chem. Sci. Eng. **15**, 998 (2021)
7. B. Gigante, Â.O. Prazeres, M.J. Marcelo-Curto, A. Comélis, P. Laszlo, J. Org. Chem. **60**, 3445 (1995)
8. M.A. Zolfigol, A. Khazaei, A.R. Moosavi-Zare, A. Zare, H.G. Kruger, Z. Asgari, V. Khakyzadeh, M. Kazem-Rostami, J. Org. Chem. **77**, 3640 (2012)
9. K. Qiao, H. Hagiwara, C. Yokoyama, J. Mol. Catal. A: Chem. **246**, 65 (2006)
10. Y.-E. Qian, L. Zheng, H.-Y. Xiang, H. Yang, Org. Biomol. Chem. **19**, 4835 (2021)
11. R. Deng, K. You, W. Ni, F. Zhao, P. Liu, H. Luo, Appl. Catal. A Gen. **594**, 117468 (2020)
12. R. Deng, K. You, F. Zhao, P. Liu, H. Luo, Can. J. Chem. Eng. **96**, 2586 (2018)
13. Y. Jiao, M. Zhu, R. Deng, J. Jian, Y. Yin, K. You, Res. Chem. Intermed. **43**, 3961 (2017)
14. J. Yan, W. Ni, K. You, T. Duan, R. Deng, Y. Chen, F. Zhao, P. Liu, H. Luo, Res. Chem. Intermed. **47**, 3569 (2021)
15. A.S. Khder, A.I. Ahmed, Appl. Catal. A Gen. **354**, 153 (2009)
16. M. Mascal, L. Yin, R. Edwards, M. Jarosh, J. Org. Chem. **73**, 6148 (2008)
17. H. Wang, X. Peng, C. Shi, X. Dong, Y. Tai, H. Liu, Res. Chem. Intermed. **40**, 1495 (2014)
18. N. Liu, X. Guo, A. Navrotsky, L. Shi, D. Wu, J. Catal. **342**, 158 (2016)
19. P.A. Alaba, Y.M. Sani, W.M. Ashri Wan Daud, RSC Adv. **6**, 78351 (2016)

20. Y. Wu, S. Liao, Front. Chem. Eng. China **3**, 330 (2009)
21. Y. Wei, W. Jiang, Y. Liu, X. Bai, D. Hao, B.-J. Ni, Nanoscale **14**, 2990 (2022)
22. M.L. Occelli, D.A. Schiraldi, A. Auroux, R.A. Keogh, B.H. Davis, Appl. Catal. A Gen. **209**, 165 (2001)
23. L.F. Córdoba, W.M.H. Sachtler, C.M. Correa, Appl. Catal. B Environ. **56**, 269 (2005)
24. P. Wang, J. Zhu, X. Liu, T. Lu, M. Lu, ChemPlusChem **78**, 310 (2013)
25. J. Yan, K. You, W. Ni, T. Duan, Z. Chen, F. Zhao, H. Luo, React. Chem. Eng. **6**, 2204 (2021)
26. Q. Chu, J. Chen, W. Hou, H. Yu, P. Wang, R. Liu, G. Song, H. Zhu, P. Zhao, Chinese. J. Catal. **39**, 955 (2018)
27. Y. Wang, H. Yuan, Z. Zhang, Y. Ke, J. Porous Mater. **27**, 429 (2019)
28. H. Wang, W. Li, J. Wang, H.-M. Chang, H. Jameel, Q. Zhang, S. Li, L. Jin, RSC Adv. **7**, 50027 (2017)
29. H.-G. Wang, G.-L. Shi, F. Yu, R.-F. Li, Fuel Process. Technol. **145**, 9 (2016)
30. H. Song, N. Wang, H.-L. Song, F. Li, Z.-S. Jin, Chin. J. Chem. Eng. **22**, 1226 (2014)
31. S. Li, H. Song, Y. Hu, F. Li, Y. Chen, Catal. Commun. **104**, 57 (2018)
32. H. Yang, R. Lu, J. Zhao, X. Yang, L. Shen, Z. Wang, Mater. Chem. Phys. **80**, 68 (2003)
33. D.A. Ward, E.I. Ko, J. Catal. **150**, 18 (1994)
34. X. Peng, N. Fukui, M. Mizuta, H. Suzuki, Org. Biomol. Chem. **1**, 2326 (2003)
35. K. You, Z. Zhou, J. Jian, R. Deng, P. Liu, Q. Ai, H. Luo, Res. Chem. Intermed. **41**, 8307 (2015)
36. D.M. Badgujar, M.B. Talawar, P.P. Mahulikar, Propell. Explos. Pyrot. **41**, 24 (2016)
37. P. Liu, W. Xiong, X. Wang, K. Huang, F. Hao, L. Wang, H. Luo, Res. Chem. Intermed. **41**, 4533 (2015)
38. M. Brandt, S. Klein, G. Wegener, US 6737554 (2004)
39. H. Wang, Y. Li, F. Yu, Q. Wang, B. Xing, D. Li, R. Li, Chem. Eng. J. **364**, 111 (2019)
40. M.Q. Al-Fahdawi, A. Rasedee, M.S. Al-Qubaisi, F.H. Alhassan, R. Rosli, M.E. El Zowalaty, S.E. Naadja, T.J. Webster, Y.H. Taufiq-Yap, Int. J. Nanomed. **10**, 5739 (2015)
41. M. Kantcheva, Appl. Catal. B Environ. **42**, 89 (2003)
42. X. Zhang, Y. Huang, J. Yang, H. Gao, Y. Huang, X. Luo, Z. Liang, P. Tontiwachwuthikul, Chem. Eng. J. **383**, 123077 (2020)
43. H.Z. Ma, F.T. Chen, B. Wang, Q.F. Zhuo, J. Hazard. Mater. **145**, 453 (2007)
44. X. Zhang, J. Hong, H. Liu, X. Luo, W. Olson, P. Tontiwachwuthikul, Z. Liang, AlChE J. **64**, 3988 (2018)
45. X. Zhang, H. Liu, Z. Liang, R. Idem, P. Tontiwachwuthikul, M.J. Al-Marri, A. Benamor, Appl. Energ. **229**, 562 (2018)
46. M. Benaïssa, J.G. Santiesteban, G. Díaz, C.D. Chang, M. José-Yacamán, J. Catal. **161**, 694 (1996)
47. L. Huang, L. Wang, Z. Zhang, X. Guo, X. Zhang, J.M. Chabu, P. Liu, F. Tang, J. Energy Chem. **71**, 225 (2022)
48. X. Zhang, Z. Zhu, X. Sun, J. Yang, H. Gao, Y. Huang, X. Luo, Z. Liang, P. Tontiwachwuthikul, Environ. Sci. Technol. **53**, 6094 (2019)
49. C. Morterra, G. Cerrato, S. Ardizzone, C.L. Bianchi, M. Signoretto, F. Pinna, Phys. Chem. Chem. Phys. **4**, 3136 (2002)
50. V. Pârvulescu, S. Coman, P. Grange, V.I. Pârvulescu, Appl. Catal. A Gen. **176**, 27 (1999)
51. S.G. Jurado, C.R. Vera, J. Mol. Catal. A Chem. **398**, 325 (2015)
52. A.L.C. Pereira, S.G. Marchetti, A. Albornoz, P. Reyes, M. Oportus, M.C. Rangel, Appl. Catal. A Gen. **334**, 187 (2008)
53. K. Ebitani, H. Konno, T. Tanaka, H. Hattori, J. Catal. **135**, 60 (1992)
54. Z. Han, M. Lv, X. Shi, G. Li, J. Zhao, X. Zhao, Adv. Fiber Mater. **5**, 266 (2023)
55. D. Hao, Y. Liu, S. Gao, H. Arandiyan, X. Bai, Q. Kong, W. Wei, P.K. Shen, B.-J. Ni, Mater. Today **46**, 212 (2021)

Publisher's Note Springer Nature remains neutral with regard to jurisdictional claims in published maps and institutional affiliations.

Springer Nature or its licensor (e.g. a society or other partner) holds exclusive rights to this article under a publishing agreement with the author(s) or other rightsholder(s); author self-archiving of the accepted manuscript version of this article is solely governed by the terms of such publishing agreement and applicable law.